Article

Chinese Science Bulletin

Environmental Chemistry

November 2011 Vol.56 No.32: 3437–3444
doi: 10.1007/s11434-011-4712-8

Evaluation of humic acid removal by a flat submerged membrane photoreactor

WEI Yong[1,2], CHU HuaQiang[1*], DONG BingZhi[1*] & LI Xuan[1]

[1] *School of Environmental Science and Engineering, State Key Laboratory of Pollution Control and Resource Reuse, Tongji University, Shanghai 200092, China;*
[2] *School of Environmental and Safety Engineering, Changzhou University, Changzhou 213164, China*

Received May 9, 2011; accepted June 14, 2011

A flat submerged membrane combined with a TiO_2/UV photocatalytic reactor (FSMPR) was employed in batch mode to remove humic acid (HA). HA removal efficiency was characterized by UV_{254} absorbance, UV-vis spectra, dissolved organic carbon (DOC) concentration, specific UV absorbance (SUVA), and trihalomethane formation potential (THMFP). The FSMPR process was effective in removing more than 86% of DOC and nearly 100% of UV_{254} absorbance, while the THMFPs of samples were reduced to < 19 μg/L after 150 min of treatment. In addition, changes in transmembrane pressure (TMP) with and without UV were evaluated; TiO_2/UV was effective at controlling membrane fouling by HA. Analysis of the molecular weight (MW) distributions and three-dimensional excitation-emission matrix (EEM) fluorescence spectra of HAs revealed that the effectiveness in membrane fouling control is a result of changes in HA molecular characteristics. The TiO_2/UV photocatalytic reactor caused the degradation of high MW, hydrophobic humic-like molecules to low MW, hydrophilic protein-like molecules, although this fraction was not completely removed during 150 min of treatment and was less responsible for membrane fouling.

TiO_2/UV, natural organic matter, membrane fouling, molecular weight distribution, excitation and emission matrix

Citation: Wei Y, Chu H Q, Dong B Z, et al. Evaluation of humic acid removal by a flat submerged membrane photoreactor. Chinese Sci Bull, 2011, 56: 3437–3444, doi: 10.1007/s11434-011-4712-8

Humic acid (HA), an important component of natural organic matter (NOM), is derived from the decomposition of the plant and animal materials that are commonly found in surface and ground water [1]. The presence of humic substances can impart an undesirable taste and color to drinking water. Humic materials can compete for adsorption sites with targeted compounds in coagulation treatments and activated carbon adsorption. They can also react with chlorine during water disinfection processes to form disinfection byproducts such as trihalomethanes, haloacetic acids, and haloacetonitriles. Therefore, control of HA plays an important role in treating surface water. Previous studies have reported that NOM with HA is difficult to remove using conventional treatment processes, with TOC removal efficiencies of only about 10%–50% [2].

Microfiltration (MF) and ultrafiltration (UF) membranes are effective in removing aquatic substances such as turbidity and pathogens but they are not effective for NOM removal; MF/UF treatment processes can achieve only nominal (10%) removal of NOM [3] and can contribute to the fouling of membranes [4], which is usually considered to be the most challenging factor in membrane applications. Therefore, pretreatment of feed water to membranes has become more important.

One of the chemical methods for HA removal is heterogenous photocatalysis. TiO_2 is the most commonly used photocatalyst because of its considerable photocatalytic activity, high stability, non-environmental impact and low cost [5]. Generally, a suspension of catalyst is used for high efficiency photocatalytic degradation and the catalyst particles must be separated from the treated water after the reaction. The combination of photocatalysis and membranes

*Corresponding authors (email: chq123zl@hotmail.com; dbz77@tongji.edu.cn)

was designed to solve the above requirements. The membrane could play the role of both a simple barrier for the photocatalyst and a selective barrier for the molecules to be degraded. Compared with conventional photoreactors, the combination of membranes with photocatalysts (membrane photocatalytic reactors, MPR) is advantageous in confining the photocatalyst within the reaction environment by the membrane, control of a residence time of molecules in the reactor and realization of a continuous process with simultaneous products separation from the reaction environment [6–10]. Therefore, the combination of two processes is commonly used for two major reasons: the enhancement of the removal of NOM, and the reduction of membrane fouling. Both reasons, in turn, influenced the cost and acceptability of membrane use [11].

There have been many studies on removal of NOM by MPR, most of which focused on the effect of treatment parameters, such as pH, TiO_2 concentration, airflow, irradiation intensity, the addition of $CaCl_2$, catalyst loading, catalyst species and initial HA concentration on removal efficiency [6,12–16]. In addition, these studies used bulk parameters, such as TOC analysis or UV spectrophotometry to assess the treatment performance and effect on membrane fouling. Although these parameters are sufficient to give a general assessment, they cannot elucidate the specific chemistry of the process.

In this study, a flat submerged membrane photocatalytic reactor was designed for the degradation of HA in batch mode at pH 7 using commercial TiO_2. Several complementary analytical methods were used to further understand the degradation process. DOC levels, UV_{254} absorbances, UV-vis spectra, SUVA values, and THMFPs of water samples were monitored over time. In addition, the MW distributions of organic matter in the samples were determined and EEM fluorescence spectra were obtained. Transmembrane pressure (TMP) was investigated to determine its affect on membrane separation performance. These measurements are important in determining the characteristics of intermediate treatment products and assessing how these products affect membrane separation processes.

1 Materials and methods

1.1 Materials

TiO_2 P25 (ca. 50 m^2 g^{-1}; 25 nm) was purchased from Degussa (Hanau, Germany). Before use, 4.0 g of TiO_2 powder was weighed and mixed with a small amount of ultrapure water to prepare a TiO_2 slurry, which was added to the photocatalytic reactor. This resulted in a TiO_2 concentration of 0.5 g/L in the mixed liquor. HA was provided by Ju Feng Chemical Technology Co., Ltd., Shanghai, China. NaOH was used to improve the dissolution of HA in water. At pH 12, 1 g of HA powder was dissolved in 100 mL of a 0.1 mol/L NaOH solution. The resultant solution was diluted to 1000 mL with deionized water (MilliQ), filtered through a 0.45 μm cellulose acetate filter membrane (Xingya Purification Material Plant, Shanghai) to remove all suspended solids, and stored at 4°C. The pH values of the solutions were adjusted by adding HCl or NaOH. All reagents utilized were of analytical purity. The initial concentration of HA used in the experiment was about 10 mg L^{-1} (DOC). The membrane module was a polyvinylidene fluoride (PVDF) flat membrane with a mean pore size of 0.08 μm and a filtration area of 0.02 m^2 and was provided by Lantian Peier Membrane Co., Ltd., China. The membrane module was treated with an ethanol/water mixture (3/97 by volume) for 24 h and rinsed with purified water to remove residual dissolved organic matter. All membrane samples were stored in purified water at 4°C and the water was replaced regularly.

1.2 Photoreactor

The FSMPR process, shown in Figure 1, was designed and conducted on a laboratory scale. The reactor was made of stainless steel and had an effective volume of 8 L. A stainless steel light baffle separated the reactor into two parts: the photocatalytic oxidation (PCO) zone and the membrane separation zone. These were connected by a bottom flow channel and an upper overflow channel. Three low-pressure UV lamps (16 W, Philip) emitting at a wavelength of predominantly 253.7 nm were suspended vertically inside a quartz glass cylinder in the middle of the PCO zone. The intensity of radiation was 1.17 mW cm^{-2}. The mixture was circulated by a recycle pump and magnetically stirred during the irradiation to ensure a homogenous mixture. Air (4 L min^{-1}) was supplied by a longitudinal air diffuser directly below the membrane module to provide good mixing and dissolved oxygen for photoreaction. The aeration also fluidized the TiO_2 particles and created sufficient turbulence along the membrane surface to avoid deposition of TiO_2 particles and to maintain the TiO_2 concentration.

During the experiments, the reaction temperature was

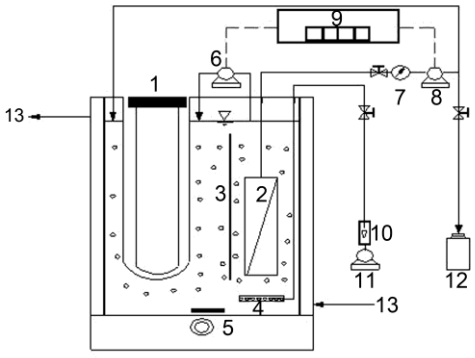

Figure 1 Schematic of the FSMPR system. 1, UV lamp; 2, flat membrane model; 3, baffle; 4, air diffuser; 5, magentic stirrer; 6, recycle pump; 7, pressure gauge; 8, effluent pump; 9, control system; 10, flow meter; 11, air pump; 12, sampling; 13, cooling water.

maintained at about 25°C with the aid of recirculating cooling water. A constant flux of permeate (40.0 L $m^{-2} h^{-1}$) was withdrawn by a peristaltic pump. The TMP in all experiments was measured by a precision pressure gauge on the permeate line. The penetrating fluid was returned to the photocatalytic reactor to keep the reactor volume constant (batch mode). Samples were taken from the permeate line at predetermined times and analyzed. To minimize the effect of adsorption, the suspension was left in the dark for 30 min before the UV light was switched on. The reaction rate constant of the photocatalytic oxidation was analyzed from 0 to 150 min.

1.3 Analytical methods

The DOC was analyzed with TOC-V_{CPH} (Shimadzu, Japan). UV_{254} absorbance and UV-vis spectra were measured by a UV-spectrophotometer (Shimadzu UV-2550, Japan). The THMFPs of samples was tested according to USEPA Method 551.1 with gas chromatography-electron capture detector (GC-ECD) (Agilent 6890N, USA) equipped with a capillary column (30.0 m × 0.32 mm × 0.25 μm, HP-5, Agilent J&W, USA).

The MW distribution was measured with the gel permeation chromatography (GPC) method on a high performance liquid chromatography (LC-10AD, Shimadzu, Japan) system coupled with an SPD-20A UV detector and a TSK-GEL G3000PWXL column (7.8 mm × 300 mm). Anhydrous sodium sulfate (0.05 mol L^{-1}) was used as the isocratic mobile phase. The separated compounds were detected by UV absorbance at 254 nm. The MW distribution pattern was derived by calibration with poly-styrene sulfonate MW standards of 14, 7.5, 4.3, 1.4, 0.7, 0.5 and 0.21 kDa. The weight and number average molecular weights (MW and MN, respectively) were calculated from the GPC results. The ratio of MW/MN or polydispersity index can be used as a measure of the width of the MW distribution.

The three-dimensional EEM spectra were measured by a fluorescence spectrophotometer (F-4600, Hitachi, Japan). In this study, the EEM spectra were collected with corresponding scanning emission spectra from 200 to 550 nm at 5 nm increments by varying the excitation wavelength. The excitation and emission slits were maintained at 10 nm and the scanning speed was set at 1200 nm/min. The software Origin 7.5 and Surfer 8.0 were employed to process the EEM data.

2 Results and discussion

2.1 Removal of HA

Figure 2(a) shows the removal of DOC and UV_{254} as a function of reaction time in the FSMPR. The initial drop in DOC and UV_{254} at 0 min may be due to TiO_2 surface adsorption. There was a slight increase in DOC concentration at 30 min. This increase was not observed in UV_{254} readings. The short-term increase in DOC after the initial removal can be explained by the release of intermediate oxidation products from the TiO_2 surface. After the initial adsorption, the adsorbed HA compounds were oxidized and transformed to intermediate oxidation products. These intermediate products, more hydrophilic than the original HA compounds as a

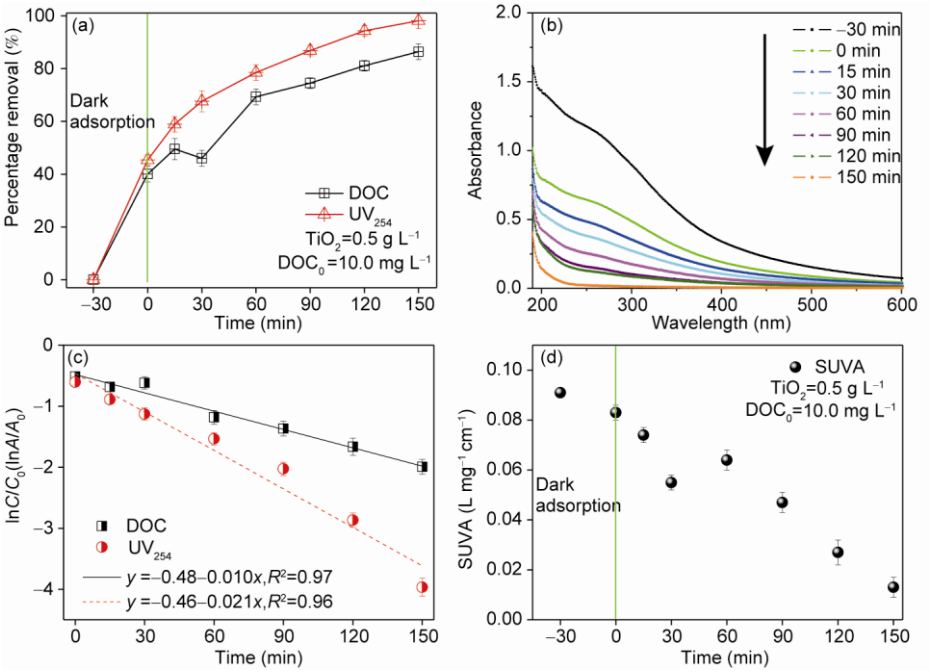

Figure 2 (color online) FSMPR treated HA with 0.5 g/L TiO_2 at pH 7 (a) removals of DOC and UV_{254}; (b) UV-vis spectra of the HA solution in photocatalytic degradation; (c) degradation kinetics of DOC and UV_{254}; (d) removal of SUVA.

result of the oxidation reaction, did not adsorb as strongly on the TiO_2 surface as the original compounds. Because the mineralization rate of the HA was less than the rate of photocatalytic degradation, release of these intermediate products from the TiO_2 surface led to an increase in DOC concentration in the solution. The decrease in DOC concentration afterwards is attributed to the mineralization of HA through photocatalytic oxidation. Figure 2(b) shows the changes in the UV-vis spectra during the degradation of HA at pH 7 in the FSMPR process. UV-vis absorbance at 190–600 nm of the HA solution continuously decreased and nearly disappeared with increased duration of photocatalysis. The initial drop at 0 min is ascribed to TiO_2 surface adsorption; after this point, any decrease in absorbance can be attributed to TiO_2 photocatalysis. TiO_2 nanoparticles can catalyze the decomposition of HA upon exposure to UV radiation. The decrease in UV-vis absorbance indicates that the intermediate decomposition products of the photocatalytic oxidation have no UV absorbance, especially at 254 nm, which confirms the above-mentioned conclusion.

The removal efficiency of UV_{254} was higher than that of DOC, with nearly 100% removal of UV_{254} and only 86% removal of DOC after 150 min treatment. The reason for this is that HA is first degraded into intermediates such as low MW organic carboxylic acids and further degraded into carbon dioxide and water [17]. The removal of DOC reflects the actual degree of mineralization of organics after the breakup of large aromatic structures. The different removal efficiencies indicate that the mineralization rate of HA was less than the rate of photocatalytic degradation. The degradation kinetics of DOC and UV_{254} during FSMPR both approximately followed a pseudo-first-order rate law, as shown in Figure 2(c). The degradation rate constants of UV_{254} and DOC were 0.021 and 0.010 min^{-1}, respectively. The apparent reaction rate constant of UV_{254} is 2.1 times that of DOC. This indicates that TiO_2 exhibited excellent photocatalytic activity for the removal of UV_{254} compared to the removal of DOC. After 150 min of treatment, approximately 1.5 mg L^{-1} residual DOC remained in the water sample, indicating that complete mineralization was not achieved. This may be due to the presence of refractory compounds in the original water sample or byproducts of oxidation. To achieve high mineralization efficiency, the durations of these photocatalytic oxidations were increased.

Specific UV absorbance (SUVA) is defined as a sample's UV absorbance at 254 nm divided by the DOC concentration of the sample. High-SUVA waters are generally rich in hydrophobic NOM, such as humic substances. SUVA values have also been found to correlate well with both the MW and aromaticity of aquatic NOM [18]. Therefore, SUVA values indicate aromatic compounds in DOC and can be used to estimate the chemical nature of the DOC at a given location. SUVA data are presented in Figure 2(d). The initial reduction in SUVA at 0 min indicates the preferred adsorption of hydrophobic HA on TiO_2. The sharp decrease in SUVA at 30 min suggests that the intermediate oxidation products released from the TiO_2 surface do not absorb significantly at 254 nm, as discussed above. After this sharp decrease, the SUVA values of the HA solution continuously decreased with reaction time. It has been reported that membrane fouling and DBP formation are closely related with SUVA [19–21]. Therefore, the reduction in SUVA suggests that the membrane fouling and DBP formation potential of the treated water should be significantly less than that of the untreated water.

In contrast, the control experiment confirmed that there was no catalytic degradation activity in the absence of light even after an extended reaction time, which is consistent with other results [13]. All changes in DOC, UV_{254}, UV-vis spectra, and SUVA values were ascribed to TiO_2 surface adsorption.

2.2 THMFP analysis

The total THMFP (TTHMFP) as a function of irradiation time was measured to assess the reactivity of degradation products with chlorine at different stages of the photocatalytic treatment. THMFP levels of HA samples subjected to different treatment times in the FSMPR process are shown in Figure 3. Only chloroform ($CHCl_3$) contributed to the total THMFP because the original HA sample had a low level of bromine. The HA sample treated for 30 min had a THMFP of 570 μg L^{-1}. In aqueous solution, chlorine is more likely to react with electron-rich sites in organic molecules such as activated aromatics (aromatic rings bearing –OH, $–NH_2$, and heterocyclic nitrogen atoms) and 1,3-dicarbonyl aliphatics [22]. Therefore, the organic structure of NOM will strongly influence the extent of chlorine consumption and THM formation. The THMFP dropped to 19 μg L^{-1} after 150 min of treatment. The effluent THMFP levels of samples subjected to 90 min of treatment met the requirement of the Chinese National Standards for Drinking Water Quality (GB5749-2006, $CHCl_3 < 60$ μg L^{-1}). This demonstrates an efficient removal of THM precursors. The low total THMFP concentration after photocatalytic treatment is consistent with the significantly reduced DOC concentration and UV_{254} absorbance after oxidation. The percentage of THMFP removal exceeds that of DOC removal, as indicated by a decrease in the specific TTHMFP (TTHMFP/DOC) from 57 to 14 μg mg^{-1}. The fraction of organic matter that forms trihalomethanes is susceptible to photocatalytic treatment. Although complete mineralization was not achieved in these experiments, photocatalytic oxidation does induce changes in the chemical structure of THM pre cursors, rendering them less reactive to chlorine [23].

2.3 Membrane performance analysis

Changes in TMP were monitored to evaluate membrane fouling. Under normal circumstances, when a certain

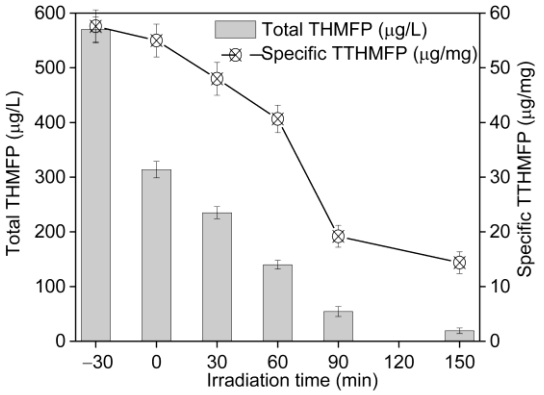

Figure 3 Total THMFP (TTHMFP) and specific TTHMFP concentration in humic acid sample before and after treatment in the FSMPR process.

membrane flux has been guaranteed, TMP should ideally be as low as possible. When TMP increases, this indicates a rise in membrane fouling resistance, which shortens the membrane wash cycle and reduces the membrane life [24]. Membrane fouling during the filtration of different solutions occurs because of the formation of a cake layer and membrane pore plugging, which leads to an increase in TMP. The resistance-in-series model was applied to evaluate fouling characteristics during a 240 min filtration. The resistances of membrane, cake layer and pore plugging were measured (Table 1). Membrane resistance is constant and depends on physical and chemical properties such as membrane thickness and morphological features. Cake resistance is mainly determined by porosity, thickness and compressibility of the cake. Pore blockage resistance depends on the amount of intruding photocatalysts or HA inside the membrane pore. According to this model, the membrane flux, J, can be expressed as follows [25–29]:

$$J = \frac{\Delta P}{\mu(R_m + R_c + R_p)}, \quad (1)$$

where J is the membrane flux (L $m^{-2} h^{-1}$), ΔP is the TMP (Pa), μ is the viscosity of permeate (Pa s), R_t is the total resistance (m^{-1}), R_m is the intrinsic membrane resistance, R_c is the cake resistance, and R_p is the fouling resistance due to pore plugging.

The TMP during filtration of the TiO_2 solution (0.5 g L^{-1}) only slightly increased initially. The resistance was caused by minor TiO_2 pore blockage resistance (0.2×10^{11} m^{-1}) and minor cake resistance (0.3×10^{11} m^{-1}). The aeration below the module may provide shearing force along the membrane surface, preventing TiO_2 particle deposition and reducing the TMP. Humic substances contained in natural waters have been demonstrated to be the foulant that causes membrane fouling in a number of studies [4,30,31]. The TMP increment rate during filtration of the HA solution (DOC_0, 10 mg L^{-1}) was 15 Pa/min. The resistance was caused by major HA pore blockage resistance (3.3×10^{11} m^{-1}) and minor cake resistance (0.2×10^{11} m^{-1}). The TMP increment rate during filtration of the HA (DOC_0, 10 mg L^{-1}) and TiO_2 (0.5 g L^{-1}) mixed solution without UV was 23 Pa/min, almost 1.54 times the rate during the filtration of the HA-only solution. The resistance was caused by major HA pore blockage resistance (2.9×10^{11} m^{-1}) and major cake resistance (2.7×10^{11} m^{-1}). Lee et al. [12] investigated the hybrid TiO_2 photocatalytic membrane reactor for HA degradation with and without ultraviolet light and illustrated the possible mechanisms of membrane fouling by TiO_2 and HA. Humic acids can occupy the vacancies between TiO_2 particles and a portion of the deposition layer resistance actually increased when the TiO_2 particles and humic acids were mixed together. Thus, humic acid-laden TiO_2 particles can be expected to give rise to a greater resistance to permeation. The cake resistance of the mixture (2.7×10^{11} m^{-1}) was more than nine times higher than the resistance due to TiO_2 alone (0.3×10^{11} m^{-1}) and more than thirteen times higher than that of HA alone (0.2×10^{11} m^{-1}). The degradation of humic acids present in suspension or bound to the TiO_2 particle surfaces played a central role in the decline of TMP when UV irradiation was provided. The TMP during filtration of the HA (DOC_0, 10 mg L^{-1}) and TiO_2 (0.5 g L^{-1}) mixed solutions with UV slightly increased initially, then remained constant throughout the rest of the filtration. The resistance was caused by minor TiO_2 pore blockage resistance (0.4×10^{11} m^{-1}) and minor cake resistance (0.6×10^{11} m^{-1}). The stabilized TMP indicates that membrane fouling did not occur and that TiO_2/UV photocatalysis was effective in controlling membrane fouling by HA.

2.4 Characteristics of MW distribution

GPC chromatograms are presented in Figure 5. The chromatogram of the initial sample at 30 min has a broad molecular weight distribution and consists mostly of large molecules (1–10 kDa), which exhibit a high response. These are typical characteristics of hydrophobic aromatic and long-chain aliphatic molecules. The MW distribution of

Table 1 Summary of resistances after 240 min for membrane filtration of different solutions

Resistance/Percentage	R_m ($\times10^{11}$ m^{-1})/(%)	R_c ($\times10^{11}$ m^{-1})/(%)	R_p ($\times10^{11}$ m^{-1})/(%)	R_t ($\times10^{11}$ m^{-1})/(%)
TiO_2	8.8/94.6	0.3/3.2	0.2/2.2	9.3/100.0
HA	9.0/71.4	0.2/1.6	3.3/26.2	12.6/100.0
HA+TiO_2	9.5/62.9	2.7/17.9	2.9/19.2	15.1/100.0
HA+TiO_2 with UV	9.6/90.5	0.6/5.7	0.4/3.8	10.6/100.0

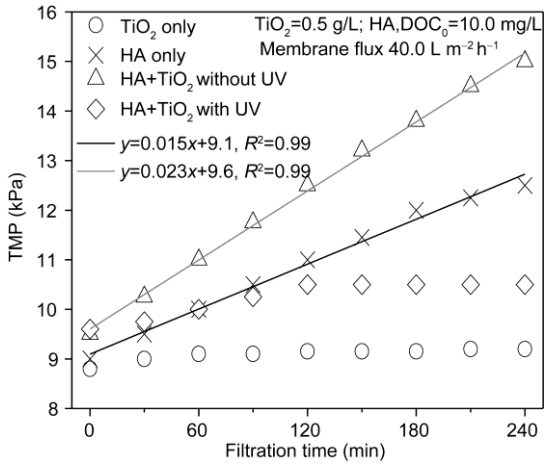

Figure 4 Changs of TMP during filtration of different solutions.

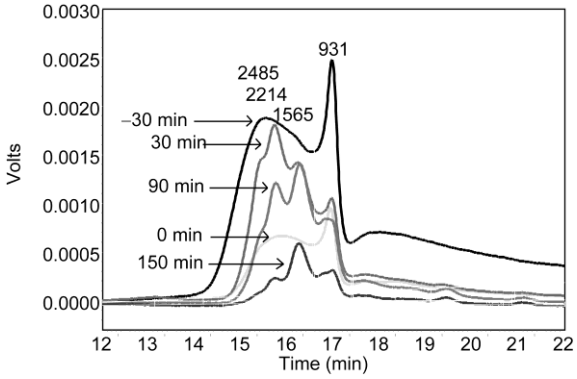

Figure 5 MW distribution of HA solution during various time treatments in the FSMPR process with 0.5 g/L TiO_2 at pH 7.

UV_{254}-active components was found to consist of two key peaks at 931 and 2485 Da. There was a decrease in the MW of HA with dark adsorption and during treatment with the FSMPR process of a 0.5 g L^{-1} TiO_2 solution at pH 7. Two peak heights decreased after 30 min of dark adsorption but the contour of MW distribution was almost unchanged. New peaks of degradation products were not found, indicating that no new intermediate compounds emerged. This removal is mainly attributed to the preferred adsorption of HA molecules (including both large and small molecular weights). In contrast, after 30 min of UV irradiation, two new peaks positioned at 2214 and 1565 Da appeared, while the peak 2485 Da continued to sharply decrease, and the peak heights of the 30 min sample were greater than those of the 0 min sample. This suggests that the intermediate oxidation products released from the TiO_2 surface were more hydrophilic than the original HA, as discussed in Section 2.1. Meanwhile, the fractions represented by the two new peaks at 2214 and 1565 Da had lower MWs than the fraction represented by the peak at 2485 Da and the fraction as a result of oxidation, represented by the peak at 1565 Da, underwent relatively little degradation after 150 min of treatment in the FSMPR. This implies that the UV/TiO_2 degradation of HA occurred through the breakage of high MW hydrophobic organic compounds to form low MW compounds, which were more hydrophilic and caused less membrane fouling. These refractory compounds could not be completely mineralized.

To better evaluate and understand MW distributions, the analysis of MN, MW and the coefficient of MW distribution(MW/MN) were investigated in this study. The MW, MN and MW/MN ratio of the initial sample were 2403 Da, 198 kDa, and 12.1, respectively, while those of samples subjected to 150 min of treatment were 1246 Da, 296 Da, and 4.2, respectively. These results indicate that the FSMPR effluent had much narrower MW distribution after treatment.

2.5 Three-dimensional EEM fluorescence spectra

Fluorescence EEMs are very useful for distinguishing between different types of organic matter [32]. In this study, photodegradation of humic substances caused great changes in the EEM fluorescence properties of humic acids and the peak intensities and positions of peaks in fluorescence EEMs obtained from treated HA samples both changed with increasing photocatalytic irradiation time. As shown in Figure 6, there were different peak positions and intensities in the fluorescence EEMs of HA solutions that had undergone different durations of treatment in the FSMPR process. The intensities of two dominant peaks, Peak A and Peak T, decreased with time in the FSMPR system, indicating that the fluorescence characteristics of HA were gradually changed with photooxidation.

The dominant excitation and emission wavelengths (*Ex*/*Em*) of 275 and 445 nm (Peak A intensity, 970.5) of the initial sample treated for 30 min (Figure 6(a)) match the excitation and emission wavelengths reported for humic

Table 2 Major fluorescent components in EEM of HA solutions during FSMPR treatment

Time (min)	Excitation/Emission (nm)	Intensity	Peak	Component type
−30	275/445	970.5	A	Humic-like
0	275/445	639.1	A	Humic-like
30	265/435	354.1	A	Humic-like
	215/330	491.7	T	Protein-like
90	260/420	139.7	A	Humic-like
	230/350	247.7	T	Protein-like
150	215/330	296.3	T	Protein-like

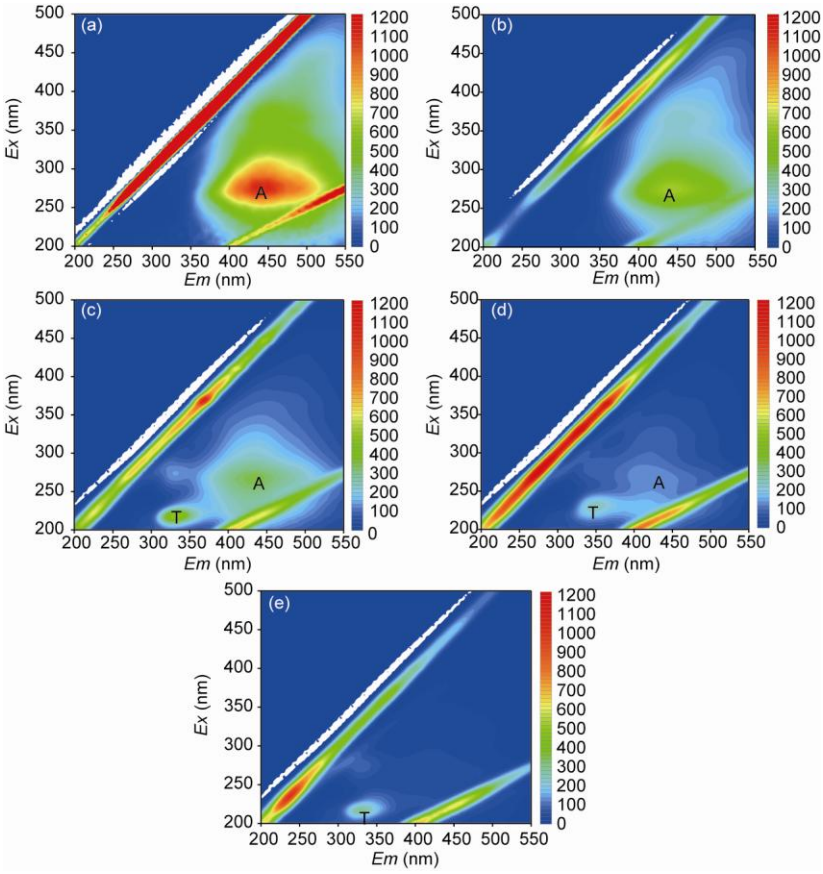

Figure 6 Fluorescence EEMs of HA solution during various time treatments in the FSMPR process with 0.5 g L^{-1} TiO_2 at pH 7. (a) –30 min; (b) 0 min; (c) 30 min; (d) 90 min; (e) 150 min.

acid-like fluorescence [18,33–35]. After 30 min of dark adsorption (Figure 6(b)), the fluorescence EEMs decreased in peak intensity (from 970.5 to 639.1) but the location of Peak A (*Ex/Em*, 275/445) was unchanged. This indicates that there was no new organic matter appearance and that TiO_2 adsorption did not change the chemical structure of HA. As shown in Figure 6(c), the Peak A intensity (*Ex/Em*, 265/435; intensity, 354.1) decreased after 30 min of photocatalysis, while a new peak, Peak T (*Ex/Em*, 215/330; intensity, 491.7), appeared. Peak T has been reported as a protein-like peak [36,37]. Both the red and blue shifts of *Ex/Em* were 10 nm. A red shift is related to the presence of carbonyl-containing substituent, hydroxyl, alkoxyl, and carboxyl groups as well as amino groups [38]. A blue shift is associated with the decomposition of condensed aromatic moieties and the breakup of large molecules into smaller fragments. This breakup may include a reduction in the degree of the π-electron system, a decrease in the number of aromatic rings, a reduction of conjugated bonds in a chain-structure, a conversion of a linear ring system to a non-linear system, or an elimination of particular functional groups including carbonyl, hydroxyl and amine groups [39–41]. The intensities of Peak A (*Ex/Em*, 260/420; intensity, 139.7) and Peak T (*Ex/Em*, 230/350; intensity, 247.7) decreased after 90 min of treatment (Figure 6(d)). Peak A disappeared and Peak T (*Ex/Em*, 215/330; intensity, 296.3) slightly increased after 150 min of treatment (Figure 6(e)), indicating that the protein-like peak fraction was due to by-products of humic acid oxidation. Based on the analysis of GPC, the presence of this fraction represented by the main peak at 1565 Da had not caused membrane fouling, as discussed in Section 2.3.

3 Conclusions

The removal of HA at pH 7 by FSMPR was investigated in batch mode using multiple analysis methods. The following conclusions can be drawn:

(1) The FSMPR process could remove more than 86% of DOC and nearly 100% of the UV_{254} absorbance of HA after 150 min treatment, as well as the effective decrease of THMFP.

(2) The TiO_2/UV pretreatment is very effective in controlling membrane fouling by HA. No remarkable increase of TMP was observed as the filtration process with the photocatalytic reactions took place.

(3) The hydrophobic humic-like molecules with high MW were degraded to hydrophilic protein-like molecules with low MW as a result of photocatalysis reaction, which

were less responsible for membrane fouling.

This work was supported by the National Water Pollution Control and Treatment Key Technologies R&D Program (*2008ZX07421-006 and 2009ZX 07424-006*).

1 Gaffney J S, Marley N A, Clark S B. Humic and fulvic acids and organic colloidal materials in the environment. Acs Sym Ser, 1996, 651: 2–16
2 Jacangelo J G, Demarco J, Owen D M, et al. Selected processes for removing nom — an overview. J Am Water Works Ass, 1995, 87: 64–77
3 Vickers J C, Thompson M A, Kelkar U G. The use of membrane filtration in conjunction with coagulation processes for improved nom removal. Desalination, 1995, 102: 57–61
4 Huang X H, Leal M, Li Q L. Degradation of natural organic matter by TiO_2 photocatalytic oxidation and its effect on fouling of low-pressure membranes. Water Res, 2008, 42: 1142–1150
5 Xi W M, Geissen S U. Separation of titanium dioxide from photocatalytically treated water by cross-flow microfiltration. Water Res, 2001, 35: 1256–1262
6 Fu J F, Ji M, Wang Z, et al. A new submerged membrane photocatalysis reactor (SMPR) for fulvic acid removal using a nanostructured photocatalyst. J Hazard Mater, 2006, 131: 238–242
7 Chin S S, Lim T M, Chiang K, et al. Hybrid low-pressure submerged membrane photoreactor for the removal of bisphenol A. Desalination, 2007, 202: 253–261
8 Chin S S, Lim T M, Chiang K, et al. Factors affecting the performance of a low-pressure submerged membrane photocatalytic reactor. Chem Eng J, 2007, 130: 53–63
9 Huang X, Meng Y, Liang P, et al. Operational conditions of a membrane filtration reactor coupled with photocatalytic oxidation. Sep Purif Technol, 2007, 55: 165–172
10 Choo K H, Chang D I, Park K W, et al. Use of an integrated photocatalysis/hollow fiber microfiltration system for the removal of trichloroethylene in water. J Hazard Mater, 2008, 152: 183–190
11 Huang H, Schwab K, Jacangelo J G. Pretreatment for low pressure membranes in water treatment: A review. Environ Sci Technol, 2009, 43: 3011–3019
12 Lee S A, Choo K H, Lee C H, et al. Use of ultrafiltration membranes for the separation of TiO_2 photocatalysts in drinking water treatment. Ind Eng Chem Res, 2001, 40: 1712–1719
13 Choo K H, Tao R, Kim M J. Use of a photocatalytic membrane reactor for the removal of natural organic matter in water: Effect of photoinduced desorption and ferrihydrite adsorption. J Membrane Sci, 2008, 322: 368–374
14 Bai H, Zhang X, Pan J, et al. Combination of nano TiO_2 photocatalytic oxidation with microfiltration (MF) for natural organic matter removal. Water Sci Technol: Water Supply, 2009, 9: 31–37
15 Xu S, Zhang X, Ng J, et al. Preparation and application of TiO_2/Al_2O_3 microspherical photocatalyst for water treatment. Water Sci Technol: Water Supply, 2009, 9: 39–44
16 Zhang X, Pan J, Fu W, et al. TiO_2 nanotube photocatalytic oxidation for water treatment. Water Sci Technol: Water Supply, 2009, 9: 45–49
17 Wiszniowski J, Robert D, Surmacz-Gorska J, et al. Photocatalytic decomposition of humic acids on TiO_2 Part I: Discussion of adsorption and mechanism. J Photochem Photobiol A, 2002, 152: 267–273
18 Leenheer J A, Croue J P. Characterizing aquatic dissolved organic matter. Environ Sci Technol, 2003, 37: 18a–26a
19 Drikas M, Chow C W K, Cook D. The impact of recalcitrant organic character on disinfection stability, trihalomethane formation and bacterial regrowth: An evaluation of magnetic ion exchange resin (MIEX (R)) and alum coagulation. J Water Supply Res T, 2003, 52: 475–487
20 Kim H C, Yu M J. Characterization of natural organic matter in conventional water treatment processes for selection of treatment processes focused on DBPs control. Water Res, 2005, 39: 4779–4789
21 Zhao Y, Taylor J, Hong S K. Combined influence of membrane surface properties and feed water qualities on RO/NF mass transfer, a pilot study. Water Res, 2005, 39: 1233–1244
22 Harrington G W, Bruchet A, Rybacki D, et al. Characterization of natural organic matter and its reactivity with chlorine. Water Disinfect Nat Org Matt, 1996, 649: 138–158
23 Liu S, Lim M, Fabris R, et al. TiO_2 photocatalysis of natural organic matter in surface water: Impact on trihalomethane and haloacetic acid formation potential. Environ Sci Technol, 2008, 42: 6218–6223
24 Xiao Y T, Xu S S, Li Z H, et al. Progress of applied research on TiO_2 photocatalysis-membrane separation coupling technology in water and wastewater treatments. Chinese Sci Bull, 2010, 55: 1345–1353
25 Belfort G, Davis R H, Zydney A L. The behavior of suspensions and macromolecular solutions in cross-flow microfiltration. J Membrane Sci, 1994, 96: 1–58
26 Ho C C, Zydney A L. A combined pore blockage and cake filtration model for protein fouling during microfiltration. J Colloid Interf Sci, 2000, 232: 389–399
27 Li H, Fane A G, Coster H G L, et al. Direct observation of particle deposition on the membrane surface during crossflow microfiltration. J Membrane Sci, 1998, 149: 83–97
28 Kim J S, Lee C H, Chang I S. Effect of pump smear on the performance of a crossflow membrane bioreactor. Water Res, 2001, 35: 2137–2144
29 Zhang X W, Pan J H, Du A J, et al. Combination of one-dimensional TiO_2 nanowire photocatalytic oxidation with microfiltration for water treatment. Water Res, 2009, 43: 1179–1186
30 Yuan W, Zydney A L. Humic acid fouling during microfiltration. J Membrane Sci, 1999, 157: 1–12
31 Howe K J, Clark M M. Fouling of microfiltration and ultrafiltration membranes by natural waters. Environ Sci Technol, 2002, 36: 3571–3576
32 Kimura K, Hane Y, Watanabe Y, et al. Irreversible membrane fouling during ultrafiltration of surface water. Water Res, 2004, 38: 3431–3441
33 Coble P G, Del Castillo C E, Avril B. Distribution and optical properties of CDOM in the Arabian Sea during the 1995 Southwest Monsoon. Deep-Sea Res Part II, 1998, 45: 2195–2223
34 Stedmon C A, Markager S. Resolving the variability in dissolved organic matter fluorescence in a temperate estuary and its catchment using PARAFAC analysis. Limnol Oceanogr, 2005, 50: 686–697
35 Stedmon C A, Markager S. Tracing the production and degradation of autochthonous fractions of dissolved organic matter by fluorescence analysis. Limnol Oceanogr, 2005, 50: 1415–1426
36 Mayer L M, Schick L L, Loder T C. Dissolved protein fluorescence in two maine estuaries. Mar Chem, 1999, 64: 171–179
37 Baker A, Inverarity R. Protein-like fluorescence intensity as a possible tool for determining river water quality. Hydrol Process, 2004, 18: 2927–2945
38 Chen J, Gu B H, Leboeuf E J, et al. Spectroscopic characterization of the structural and functional properties of natural organic matter fractions. Chemosphere, 2002, 48: 59–68
39 Coble P G. Characterization of marine and terrestrial DOM in seawater using excitation emission matrix spectroscopy. Mar Chem, 1996, 51: 325–346
40 Swietlik J, Dabrowska A, Raczyk-Stanislawiak U, et al. Reactivity of natural organic matter fractions with chlorine dioxide and ozone. Water Res, 2004, 38: 547–558
41 Korshin G V, Kumke M U, Li C W, et al. Influence of chlorination on chromophores and fluorophores in humic substances. Environ Sci Technol, 1999, 33: 1207–1212